FULL PAPER

# Dual-Targeting Lactoferrin-Conjugated Polymerized Magnetic Polydiacetylene-Assembled Nanocarriers with Self-Responsive Fluorescence/Magnetic Resonance Imaging for In Vivo Brain Tumor Therapy

*Jen-Hung Fang, Tsung-Lang Chiu, Wei-Chen Huang, Yen-Ho Lai, Shang-Hsiu Hu, You-Yin Chen,* and San-Yuan Chen**

**Maintaining a high concentration of therapeutic agents in the brain is difficult due to the restrictions of the blood–brain barrier (BBB) and rapid removal from blood circulation. To enable controlled drug release and enhance the blood–brain barrier (BBB)-crossing efficiency for brain tumor therapy, a new dual-targeting magnetic polydiacetylene nanocarriers (PDNCs) delivery system modified with lactoferrin (Lf) is developed. The PDNCs are synthesized using the ultraviolet (UV) cross-linkable 10,12-pentacosadiynoic acid (PCDA) monomers through spontaneous assembling onto the surface of superparamagnetic iron oxide (SPIO) nanoparticles to form micelles-polymerized structures. The results demonstrate that PDNCs will reduce the drug leakage and further control the drug release, and display self-responsive fluorescence upon intracellular uptake for cell trafficking and imaging-guided tumor treatment. The magnetic Lf-modified PDNCs with magnetic resonance imaging (MRI) and dual-targeting ability can enhance the transportation of the PDNCs across the BBB for tracking and targeting gliomas. An enhanced therapeutic efficiency can be obtained using Lf-*Cur* (Curcumin)-PDNCs by improving the retention time of the encapsulated *Cur* and producing fourfold higher *Cur* amounts in the brain compared to free *Cur*. Animal studies also confirm that Lf targeting and controlled release act synergistically to significantly suppress tumors in orthotopic brain-bearing rats.**

## 1. Introduction

Malignant glioma is the most aggressive brain tumor.[1] Several conventional therapies such as surgery, adjuvant radiation therapy, and chemotherapy have been used to treat cancer cells after the exact tumor has been diagnosed, but the prognosis is poor because of fast infiltration and disruption of the architecture of normal tissue.[2] Recently, several types of nanocarriers have been developed to treat brain tumors such as liposomes, carbon nanotube, micelle, and nanocapsule.[3] Nevertheless, unstable structure, high leakage of drugs, and difficultly entering the blood–brain barrier (BBB) limit the usage of vesicles for treating brain tumors.[4] Accordingly, the development of an efficient drug delivery system that can maintain a stable nanocarrier structure, and easily transport drug across the BBB to target brain glioma, is an impending mission for research workers.[5]

Recently, polymerized polydiacetylene micelles were reported for imaging and drug delivery and they demonstrated a higher stability and drug loading than a nonpolymerized counterpart or liposomes.[6] In addition, 10,12-pentacosadiynoic acid (PCDA) molecules are generally nontoxic and enable polymerization for the formation of a strong layer to reduce leakage of antitumor drugs and achieve controlled drug release.[7] Previous studies on this polydiacetylene have focused

Dr. J.-H. Fang, Prof. S.-H. Hu
Department of Biomedical Engineering and Environmental Sciences
National Tsing Hua University
Hsinchu 300, Taiwan
Dr. T.-L. Chiu
Department of Neurosurgery
Tzu Chi General Hospital
Tzu Chi University
Hualien 970, Taiwan
Dr. W.-C. Huang
Department of Materials Science and Engineering
Carnegie Mellon University
No. 5000 Forbes Avenue, Wean Hall 3325, Pittsburgh, PA 15213, USA
Dr. Y.-H. Lai, Prof. S.-Y. Chen
Department of Materials Science and Engineering
National Chiao Tung University
No. 1001, Ta-Hsueh Road, Hsinchu 300, Taiwan
E-mail: sanyuanchen@mail.nctu.edu.tw
Prof. Y.-Y. Chen
Department of Biomedical Engineering
National Yang Ming University
Sec. 2, Linong Street, Taipei 112, Taiwan
E-mail: irradiance@so-net.net.tw

DOI: 10.1002/adhm.201500750

primarily on biosensors because they display a higher sensitivity and color change in response to temperature and pH value due to molecular perturbations.[8] These recent advances have prompted us to research the potential of a novel carrier system composed of polymerized PCDA molecules and superparamagnetic iron oxide (SPIO) nanoparticles for imaging, drug delivery, and targeting.

In addition, some studied report that Curcumin (*Cur*), a natural phenolic compound found in the rhizomes of turmeric (Curcuma longa), is able to slow or stop the growth of glioma brain cancer cells and even induces apoptosis through diverse mechanisms.[9] Because of its blocking NFκB, which is the transcriptional factor for the ATP-dependent efflux pump (P-glycoprotein, P-gp) that exists both on the surface of the BBB and in glioma cells, *Cur* was the best candidate as the drug model and employed in our drug nanocarriers here.[10] Furthermore, lactoferrin (Lf) was used to target and cross into the BBB instead of transferrin (Tf). Despite the fact that Tf is a well-known pilot molecule in drug delivery systems, the saturated cellular TfR is an inferior candidate compared to Lf.[11] So far, many studies have found that the Lactoferrin receptor (LfR) not only exists on the BBB, but also on the cell surface of glioblastomas.[12] Accordingly, if the drug nanocarriers can be modified with Lf-targeting ligand, they might enhance the transport of drugs across the BBB, as well as the accumulation of nanocarriers in the brain through receptor-mediated transcytosis and endocytosis.[13]

In this study, we proposed a newly designed nanocarrier named PDNCs made from the self-assembly of polymerized magnetic PCDA micelles as an efficient drug delivery platform where the hydrophobic SPIO nanoparticle is used as a nanosubstrate for spontaneous assembling of diacetylene monomer, 10,12-pentacosadiynoic acid, on its surface through strong ionic interaction and hydrogen bonding under the ultraviolet (UV) irradiation. At the same time, the hydrophobic antitumor drug molecules can be incorporated within the shell between SPIO and PCDA. The PDNCs can overcome the disadvantage of liposomes/micelles to achieve minimal release of the drug before reaching the target site because the ionic interaction and hydrogen bonding at the SPIO surface will restrict the dynamics of alkyl side chains, which in turn drastically affects its drug release behaviors in the polymerized magnetic PCDA micelles. In addition, PCDA amphiphiles with stimuli-responsive fluorescence upon cellular uptake can be used for trafficking the nanocarriers. Furthermore, the use of Lf ligands enables transportation across the BBB, and also targets brain tumors. The drug distribution in the plasma and brain of rate and therapeutic effect were further evaluated in vivo in neuro-oncology experiments through systemic administration.

## 2. Results and Discussion

### 2.1. Synthesis of Superparamagnetic Iron Oxide (SPIO) Nanoparticles and Polydiacetylene-Based Nanovehicles (PDNCs)

The schematic diagram in **Figure 1** illustrates the synthesis of *Cur*-PDNCs (PDNCs loaded *Cur*) by emulsion and UV irradiation process. The PCDA molecules with diacetylene group

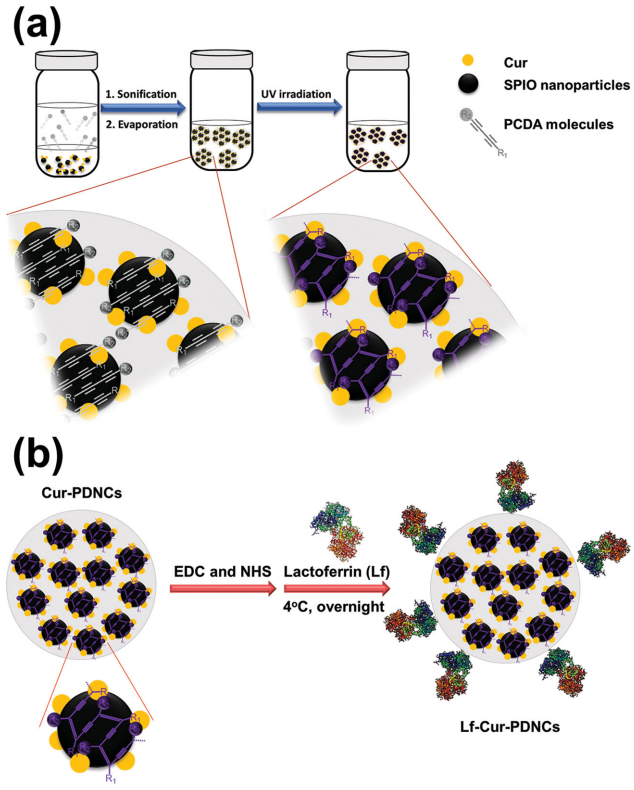


**Figure 1.** a) Flow diagram for synthesis of drug nanocarriers. PVA, PCDA, and SPIO nanoparticles were emulsified under sonication. After the solvent was vaporized at RT for 4 h, the products were treated with UV irradiation to form PDNCs. b) Process of modifying PDNCs with Lf through EDC and NHS.

can be self-assembled on the SPIO nanoparticles and polymerized to connect with other molecule chains under UV irradiation at a wavelength of 254 nm as shown in Figure 1a. During the process, the *Cur* drug molecules can be intercalated in between PCDA molecules and SPIO nanoparticles by absorption on the hydrophobic surface of the SPIO nanoparticles.[14] The SPIO nanoparticles-*Cur*-PCDA micelle units can be tightly stacked into *Cur*-PDNCs assembling structure, and stabilized by surfactant amphiphilic PVA. With this construction, we can reduce the drug leakage that occurs in the micelle or liposome structure. The SPIO nanoparticles in the nanocarriers not only act as a stabilizer to maintain the structure, but also as a contrast agent for biomedical imaging and magnetic guidance for tumor treatment in the body. Subsequently, the lactoferrin (Lf) ligands were conjugated on the PDNCs as dual-targeting ligand to transport therapeutic agent (*Cur*) across the BBB (Grade I targeting) and target brain tumor cells (Grade II targeting) as shown in Figure 1b.

The SPIO nanoparticles were synthesized through high-temperature solution phase reaction by means of heating $Fe(acac)_3$, 1,2-hexadecanediol, oleic acid, oleylamine, and benzyl ether to 285 °C. The size of the oleic acid-stabilized SPIO nanoparticles was uniform at 5–7 nm as determined by TEM as shown in **Figure 2**a. SEM image showed that the PDNCs displayed nearly homogenous spherical nanoparticles with the particle size distribution around 100–120 nm as confirmed by DLS in

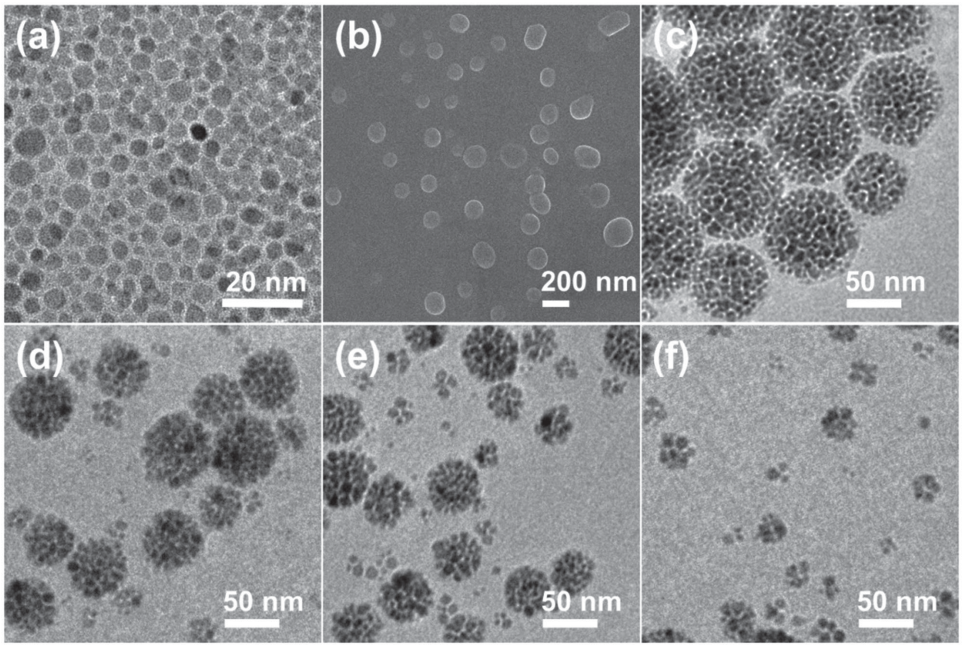


**Figure 2.** a) TEM images of SPIO nanoparticles with sizes around 5–7 nm. b) SEM images of PDNCs fabricated with 2.4 mg SPIO nanoparticles. TEM image of PDNCs fabricated with various concentration of SPIO nanoparticles: c) 2.4 mg, d) 1.2 mg, e) 0.6 mg, and f) 0.12 mg.

Table S1 (Note 1 in the Supporting Information), when 2.4 mg SPIO nanoparticles were added during the synthesis procedure (Figure 2b,c). TEM images showed that the PDNCs presented a "custard apple-like assembling structural" morphology with SPIO nanoparticle-PCDA micelles stacked tightly and stabilized by surfactant PVA. Furthermore, it was found that as decreasing the amount of SPIO nanoparticles during the emulsification process, the particle size of the PDNCs also decreased. As illustrated in Figure 2d–f, when SPIO nanoparticles of 1.2, 0.6, and 0.12 mg were added during the synthesis procedure, the PDNCs displayed smaller and less uniform size, indicating that the SPIO nanoparticles play a role in stabilizing the nanocarriers. Furthermore, it was noted that without assistance of SPIO nanoparticles, the nanocarriers cannot be conformed via the emulsion process even in the presence of PVA surfactant. Hence, it was the key to use both PVA and SPIO nanoparticles as the stabilizing agents to manufacture the PDNCs in this study.

Furthermore, we found that the concentration of SPIO nanoparticles in PDNCs was correlated with the EE% and loading amount of *Cur*, as shown in **Table 1**. As mentioned above, a minimum concentration of SPIO nanoparticles was required to form stable PDNCs with more hydrophobic cargos to encapsulate more *Cur* in the PDNCs. In PDNCs with 2.4 mg SPIO nanoparticles, the *Cur* amount (about 2 mg) was almost completely encapsulated in the cargos, but with 0.12 mg SPIO nanoparticles, only 5.1% (about 0.1 mg of *Cur*) was encapsulated.

**Table 1.** Concentration of SPIO nanoparticles and EE of *Cur* in PDNCs.

| SPIO nanoparticles in PDNCs | EE% |
|---|---|
| 2.4 mg | 90.3 |
| 1.2 mg | 48.6 |
| 0.6 mg | 38.3 |
| 0.12 mg | 5.1 |

Another important characteristic of PDNCs is the fact that the nanocarriers can be crosslinked among the PCDA molecules under 254 nm UV irradiation for 0.1, 0.5, 1, 5, and 10 min. According to Beer's law, the value of optical density (OD value) is proportional to the intensity of the changing color in the dilute solution, i.e., the degree of polymerization in UV.[15] The absorption intensity of the peak at 650 nm increased with longer irradiation time (Figure S1, Note 2 in the Supporting Information) because the PCDA molecule chain connected with another PCDA molecule chain in PDNCs (the concentration of ene-yne-conjugated backbone increases) to form a strict structure. Detailed information can be referred to Note 3 in the Supporting Information. As a result, as the exposure to UV irradiation increased, the PDNCs structure became stricter and the color deepened. This concept can be applied to modulate the drug release of PDNCs.

### 2.2. Drug Release

For the drug release study, we detected *Cur* release from polymerized *Cur*-PDNCs at a specific time by HPLC. The drug release of free *Cur* and *Cur*-PDNCs in **Figure 3** demonstrates that free *Cur* was released within 10 h, but the cumulative *Cur* release encapsulated in the *Cur*-PDNCs was reduced. In addition, we found that the *Cur* release from the *Cur*-PDNCs was significantly decreased as the UV irradiation time increased because of the increase in the degree of polymerization (the number of monomeric units in a molecule). In other words, UV irradiation formed a conjugated backbone that linked PCDA

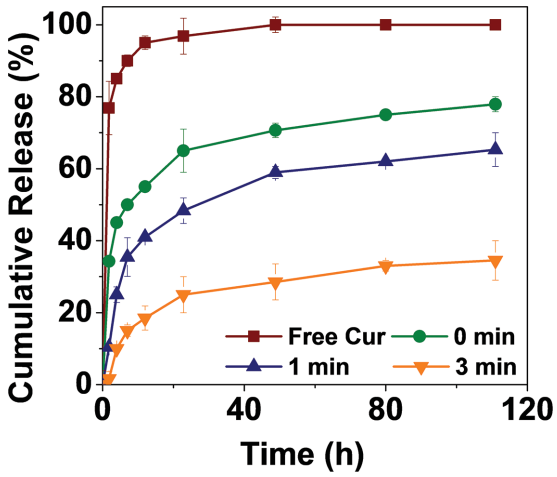


**Figure 3.** In vitro natural release of free *Cur* and *Cur*-PDNCs after treatment with UV irradiation for 0, 1, and 3 min.

molecules by covalent bonds with a polymeric structure and blocked the release channels for drugs in the nanocarriers.[16] The cumulative drug release was only about 30% in *Cur*-PDNCs treated with UV for 3 min within the first 2 d and was lower than that in other groups. The results demonstrate the successful construction of a controlled drug release system using photo polymerization of PCDA molecules.

### 2.3. Cell Compatibility and Cytotoxicity

Since we encapsulated *Cur* in PDNCs by emulsification and then polymerized the nanoparticles by UV irradiation, the activity of *Cur* needs to be examined. Detailed process was shown in Note 4 in the Supporting Information. Our results confirmed that UV irradiation does not affect the cytotoxicity of *Cur* on RG2 cells. The effect of PDNCs on cell viability of RG2 cells needs to be fully understood. Here we tested the cytotoxicity of the DNCs (before crosslinking by UV irradiation) and PDNCs (after polymerized and crosslinking by UV irradiation) on RG2 cells incubated for 24 h with increasing concentration from 25 to 1000 μg $mL^{-1}$. The results as shown in **Figure 4**a demonstrated that PDNCs display high biocompatibility and low toxicity with cell viability. In Figure 4b, both *Cur*-PDNCs and Lf-*Cur*-PDNCs incubated with RG2 cells at various times demonstrated that Lf-PDNCs displayed a higher toxicity on the RG2 cancer cells because of the targeting effect and easy uptake into RG2 cells through endocytosis.

### 2.4. Cell Uptake Efficiency

One of the goals for cancer treatments is the targeted delivery of sufficient amounts of anticancer drugs in order to minimize side effects and damage to normal tissues. Moreover, a high intracellular drug level is important, so the high selectivity for tumor tissues is a primary concern when designing a drug delivery system. We coupled Lf to PDNCs to enhance the efficiency of cell uptake with the help of EDC and NHS, where the carboxylic acid group on the surface of PDNCs connects with the amine group on the end of Lf by covalent bonding in the presence of the catalysts, EDC and NHS. We used Fourier transform infrared (FT-IR) spectrum to determine the connection between Lf and PDNCs as shown in Figure S4 (Detailed information can be referred to Note 5 in the Supporting Information). FT-IR spectrum analysis of the Lf-PDNCs revealed new peaks at 1658 $cm^{-1}$ and 1540 $cm^{-1}$, which were attributed to the stretching of the carbonyl groups in the amide bonds of Lf; these peaks were not present in the spectrum of the PDNCs alone. The strong peak at 1735 $cm^{-1}$ and the broad peak at 3354 $cm^{-1}$ were attributed to carbonyl bond stretching and hydroxyl group stretching in carboxylic acid, respectively. In addition, the peak at 2920 $cm^{-1}$ showed the carbon–carbon single bond stretching of the PVA in the PDNCs. More importantly, the PCDA molecules with remarkable stimuli-responsive and nonlinear optical properties can be used as potential sensors or detectors to display color responses in the field of biological detection. **Figure 5**a shows the fluorescence images of cell uptake after incubating PDNCs as well as Lf-PDNCs in RG2 cells for 4 h. We found that only a few PDNCs could enter into RG2 cells through endocytosis since there are no functional groups overexpressed on the PDNCs. In contrast, there were many red spots appearing in RG2 cells while PDNCs were modified with Lf (Lf-PDNCs). The red fluorescence resulted from the structural perturbations of PCDA molecules during the cell uptake reaction of Lf-PDNCs because no fluorescence molecules were conjugated to the carriers, The ene-yne-conjugated backbone in the PCDA would bear high strain under the uptake process of PDNCs to the tumor cells that was caused by plasma membrane and the low pH value in the endosome.[17] Without loading or labeling fluorescence molecules, the self-responsive colorimetric change in the PDNCs can be used for intracellular trafficking and furthermore as imaging-guided tumor treatment, which is an important characteristic and advantage of the PDNCs. We believed that this is the first report to demonstrate that the PDNCs constructed with SPIO/PCDA

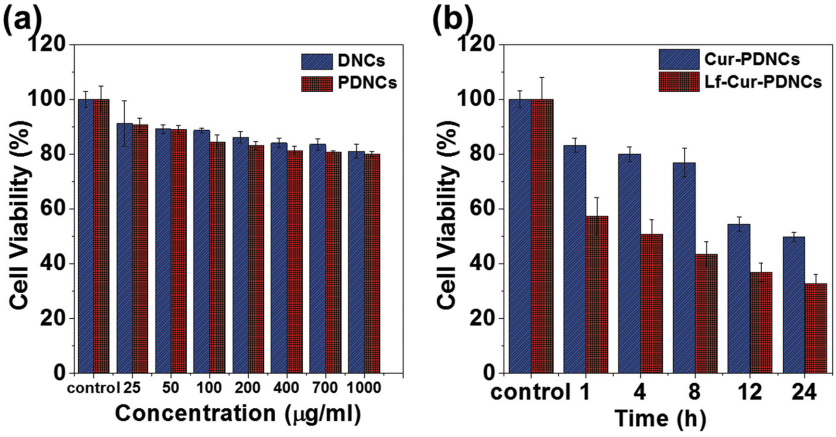


**Figure 4.** Effect of nanocarriers on cell viability of RG2 cells a) before (DNCs) and after (PDNCs) treated with UV irradiation for 1 min. b) *Cur*-PDNCs as well as Lf-*Cur*-PDNCs.

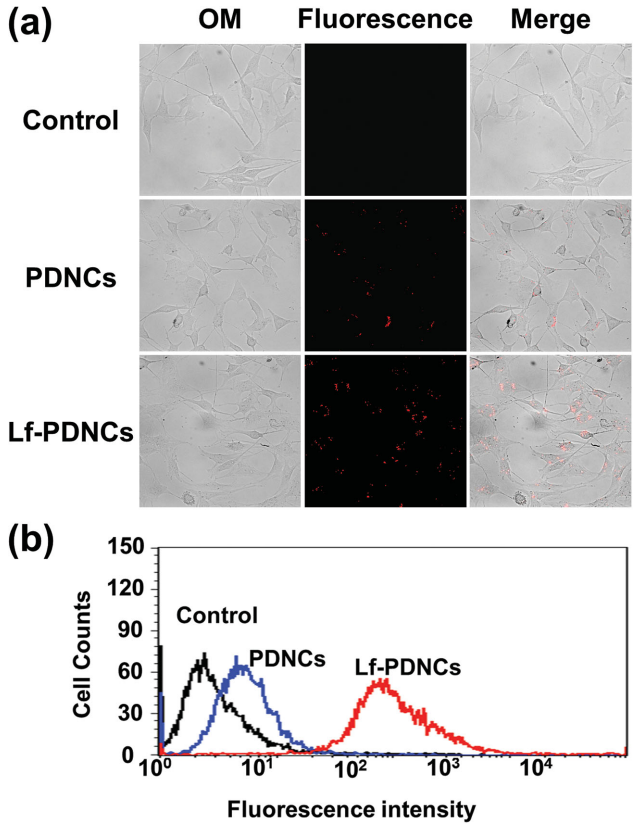


**Figure 5.** a) Fluorescence image of uptake behaviors in RG2 cells. PDNCs and Lf-PDNCs incubated with RG2 cells for 4 h. Red fluorescence spots are attributed to the perturbed structure of PCDA. b) Flow cytometry analysis of cell uptake efficiency. The curve shifted to high intensity, indicating the accumulation of Lf-PDNCs on RG2 cells over time. The horizontal axis represents fluorescence intensity, and vertical axis represents the counts of cell.

unit micelles can display self-responsive color change upon cellular uptake. Flow cytometry was further used to quantify the amounts of Lf-PDNCs in Figure 5b, showing that the fluorescence intensity increased while PDNCs were conjugated with Lf, which means more Lf-PDNCs entered cells due to enhanced peptide-mediated targeted uptake of Lf-PDNCs by cells through endocytosis. These findings demonstrate the potential use of Lf-PDNCs for active targeting, tumor imaging, and controlled drug delivery.

### 2.5. Effects on the Survival of Orthotopic Brain Tumor-Bearing Rat

To compare the BBB-crossing efficiency, in vivo magnetic resonance imaging (MRI) was performed with glioma-bearing F344 rats after injection with PDNCs or Lf-PDNCs. The upper and bottom row of horizontal $T_2$* weighted MR images in **Figure 6**a show the changes in MRI signal intensity in brain tumors 1, 24, and 72 h postinjection of PDNCs and Lf-PDNCs, respectively. Higher contrast of the brain glioma was observed with Lf-PDNCs between 1 h and 72 h after injection, but MRI with PDNCs showed no strong $T_2$* contrast enhancement at 72 h after injection. The decrease in MRI signal intensity in tumors was 58%–78% with Lf- PDNCs, as compared with the PDNCs-contrasted tumors at 72 h after injection. The Lf receptor has been shown to be overexpressed in glioma,[18] which enhanced the BBB-crossing efficiency after injection of Lf-conjugated PDNCs and caused a significant increase in the amount of Lf- PDNCs around the vascular region of the brain tumor tissue.

Figure 6b,c shows free *Cur* passage across the BBB of rats. Passage across the BBB was not surprising because it had been reported in previous studies.[19] However, free *Cur* is unstable in aqueous media[20] and presents poor bioavailability with low absorption and rapid metabolism following delivery through parenteral route[21] or intraperitoneal/ intravenous injection.[22] The encapsulation of *Cur* in the PDNCs might increase the drug bioavailability.[23] In this study, higher *Cur* concentrations were found in brain tissues following injection of *Cur*-encapsulated PDVA as compared with injection of free *Cur*. The Lf-*Cur*-PDNCs had about fourfold increase in penetration, and longer halftime in the bodies compared to free *Cur*. This formulation of Lf-*Cur*-PDNCs was specifically designed to enter the BBB and result in a higher concentration of *Cur* in the brain tumor mass in comparison to any other *Cur* formulation.

The treatment of orthotopic tumor-bearing rats is shown in **Figure 7**. After 12 d, we treated the four groups with saline, free *Cur*, Lf-PDNCs, and Lf-*Cur*-PDNCs, respectively, via tail vein injection. The dosage of *Cur* in Lf-*Cur*-PDNCs was 12 mg $kg^{-1}$ and the concentration was equivalent to that of free *Cur*. On the 21st d, three rats per group were randomly sacrificed for the histological analysis of tumor volumes, as shown in Figure 7a. The histological data showed that the tumor volumes in the *Cur*-PDNCs and Lf-*Cur*-PDNCs-treated group were smaller than those in the saline- and free *Cur*-treated groups. For statistical analysis of tumor volume for the treated groups compared with the untreated group as shown in Figure 7b, the brain tissues of the saline- and free *Cur*-treated group were seriously destroyed by cancer cells and the mean tumor volumes at days 21 were 213.5 ± 6.1 $mm^3$ ($N = 3$) for the saline-treated group versus 190.4 ± 2.8 $mm^3$ ($N = 3$) for the free *Cur*-treated group, which represents a significant differences ($p > 0.05$). There were significant declines in tumor volume for the *Cur*-PDNCs-treated (78.4 ± 2.5 $mm^3$; $p < 0.05$, $N = 3$) and Lf-*Cur*-PDNCs-treated (22.2 ± 3.2 $mm^3$; $p < 0.01$, $N = 3$) groups compared with the saline or free *Cur*-treated group. Life-span extension in Figure 7c shows that the average survival time of the Lf-*Cur*-PDNCs group was longer than that of the control group. However, *Cur*-PDNCs treatment significantly prolonged the animal survival in comparison to other treatment groups.

## 3. Conclusion

In summary, we have successfully developed a novel polymerized magnetic PDNCs as a drug delivery system synthesized by a simple emulsion process with PCDA-based micelles containing SPIO nanoparticles in the core to effectively decrease the progression of brain tumors in vivo. The PDNCs not only reduce drug leakage but also enable controlled drug release by modifying PDNCs polymerization under UV irradiation. The PDNCs with the PCDA monomers coupled on SPIO can

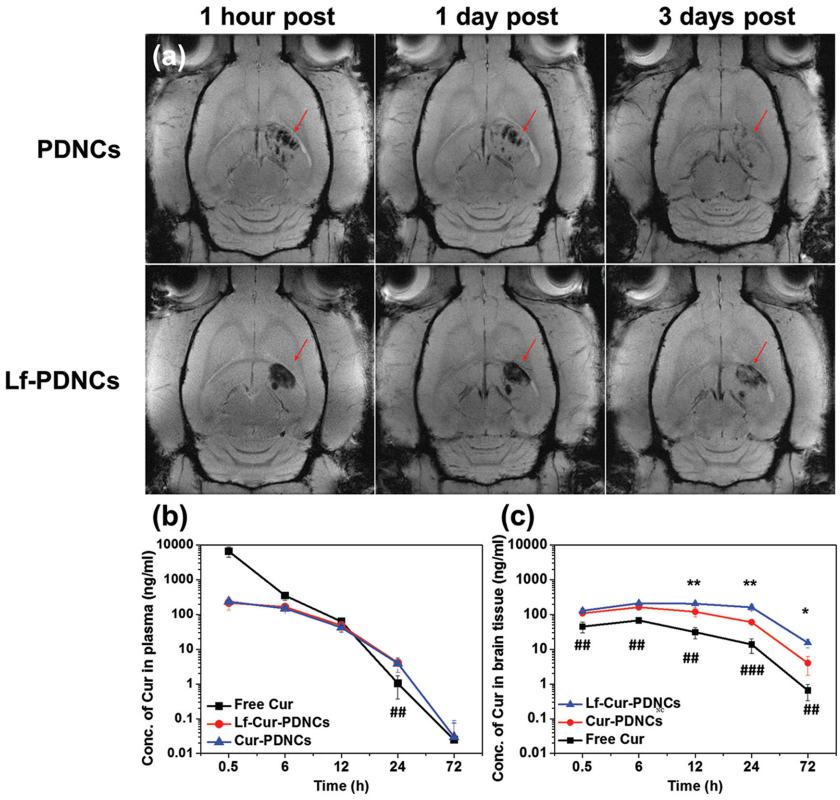


**Figure 6.** a) Series horizontal $T_2$* MR images show the accumulations of PDNCs (upper row) and Lf-PDNCs (bottom row) in brain tumors at 1 h, 1 d, and 3 d postinjection. Red arrows highlight the accumulations of nanocarriers in the brain tumors. Comparison of concentration-time profile of *Cur* in b) rat blood plasma and c) brain tumors after treating with free *Cur*, Lf-*Cur*-PDNCs and *Cur*-PDNCs, respectively. Data are expressed as mean ± SEM. $^{*}p < 0.05$ and $^{**}p < 0.01$ versus *Cur*-PDNCs; $^{\#}p < 0.05$, $^{\#\#}p < 0.01$, and $^{\#\#\#}p < 0.001$ versus free *Cur*.

display strong self-responsive color changes upon cellular uptake, which can be used for internalization and intracellular trafficking of the PDNCs without fluorescent labeling. The magnetic Lf-modified PDNCs with dual-targeting abilities can enhance the transportation of the PDNCs across the BBB and target glioma through receptor-mediated endocytosis. When rats implanted with orthotopic tumor were treated with Lf-*Cur*-PDNCs, we found the tumor size decreased in the brain and the animal survival was prolonged by about 30% in life-span compared to that of rats treated with saline or free *Cur*. We believe that Lf-*Cur*-PDNCs will be a powerful antitumor prescription in the future.

## 4. Experimental Section

*Preparation of Superparamagnetic Iron Oxide (SPIO) Nanoparticles*: We synthesized 5 nm SPIO nanoparticles following the method developed by Sun et al.[24] Briefly, 2 mmol $Fe(acac)_3$, 10 mmol 1,2-hexadecanediol, 6 mmol oleic acid, and 6 mmol oleylamine were mixed, and dissolved in 20 mL benzyl ether under magnetically stirring. Then we refluxed them in 100 °C for 30 min in a flow of nitrogen situation to remove water and oxygen. Next, the liquid was heated to 200 °C for 30 min and heated to 285 °C for another 30 min. After black-brown mixture was cooled to room temperature (RT), the product was collected by centrifugation at 3219 g for 10 min for three times and preserved it into ethanol in 4 °C.

*Synthesis of Magnetic Drug Nanocarriers*: To synthesize PDNCs, we dispersed SPIO nanoparticles at concentration of 0.12, 0.6, 1.2, and 2.4 mg to 1 mL dichloromethane, and then added 0.75 mg PCDA to form an organic phase. On the other hand, by 50 mg of 10 kDa polyvinyl alcohol (PVA) was dissolved in 2.5 mL $H_2O$ to form water phase. Next, the organic phase was added into the water phase, and emulsified by sonication for 30 s at frequency of 20 kHz and power of 130 W. The mixture was stirred magnetically in room temperature to evaporate the organic solvent. After evaporating the organic phase, the products (DNCs, diacetylene nanocarriers) were washed by the deionized water for three times, and centrifuged at 3219 g to collect the products. Then, the products were polymerized by UV irradiation under 254 nm for 1 min (40 W) to form the nanocarriers product named as PDNCs after washing by the phosphate buffered saline (PBS) for three times.

In this study, *Cur* was used as a model to estimate the drug behaviors of cancer cell therapy. Since *Cur* is a hydrophobic drug, we encapsulated

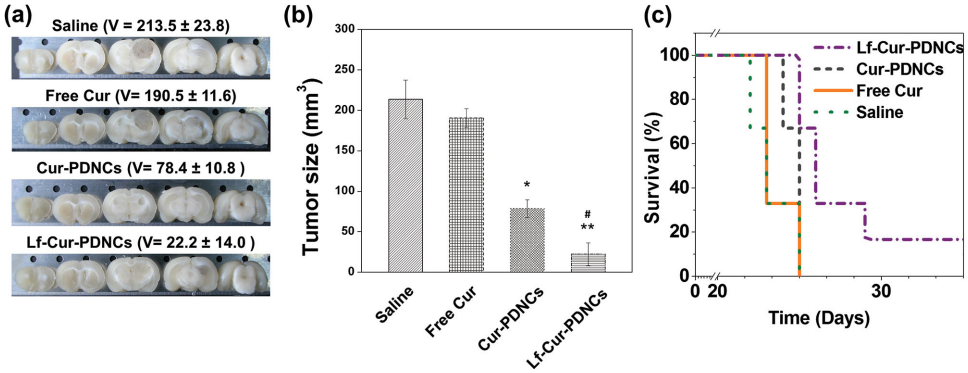


**Figure 7.** a) Representative serial photographs of the histological slices and b) statistical analysis of tumor volume for tumor-bearing rats treated with saline, free *Cur*, Cur-PDNCs, and Lf-*Cur*-PDNCs, respectively, on the 21th day ($N = 3$, each group). $^{*}p < 0.05$ and $^{**}p < 0.01$ versus free *Cur*. $^{\#}p < 0.05$ versus *Cur*-PDNCs. c) Percentage of survival (Kaplan–Meier plot) of tumor-bearing rats treated with saline, free *Cur*, *Cur*-PDNCs, and Lf-*Cur*-PDNCs, respectively. Survival was monitored daily.

it with SPIO nanoparticles in oil phase to study the drug behavior. *Cur*-loaded PDNCs (*Cur*-PDNCs) were prepared by dissolving 2 mg *Cur* into 1 mL organic phase with SPIO nanoparticles and PCDA. Then, organic phase was added into 2.5 mL water phase with PVA molecules. After we emulsified the mixture by sonicator under same condition and removing organic solvent at room temperature (RT), *Cur* was encapsulated into hydrophobic region. Subsequently, *Cur*-PDNCs were irradiated with UV for different time period (0–10 min), and preserved in PBS in 4 °C.

*Characterization*: The morphology of PCDA-based drug nanocarriers was observed by field-emission scanning eletron microscope (FE-SEM; JSM-6700F, JEOL Ltd., Tokyo, Japan), and the structure of magnetic nanoparticles as well as PDNCs was analyzed by transmission electron microscopy (TEM; JEM-2100-F, JEOL Ltd., Tokyo, Japan). For SEM analysis, PDNCs were dried on the silicon wafers, and coated with an ultrathin metal layer through the platinum sputtering to enhance the image quality taken in the experiments. For TEM analysis, PDNCs were dried on the gold grid and imaged by taking digital pictures of several locations on the grid to obtain a representative set of images. Dynamic light scattering (DLS; BI-200SM, Brookhaven instruments Corp., Holtsville, NY, USA) was used to determine the particle size and distribution of PDNCs.

*Encapsulation Efficiency (EE) and Drug Release*: High-performance liquid chromatography (HPLC, 1200 series, Agilent Technologies, Santa Clara, CA, USA) equipped with a 4.6 × 150 mm inertsil 5 μm ODS-4 column was employed to identify and quantify *Cur* with a UV detector set at the wavelength of 425 nm. After CUR was encapsulated in the PDNCs, the concentration of CUR in the supernatant could be collected by centrifugation and determined by high performance liquid chromatography (HPLC).[25] An aliquot of 10 μL of the supernatant solution was injected into the HPLC for CUR analysis. The mobile phase consisting of 35% $H_2O$ and 65% acetonitrile (ACN) was delivered at 1 mL $min^{-1}$ on an Agilent Zorbax column (C18, particle size 5 μm, 4.6 mm × 150 mm). The concentration of CUR was determined by the calibration curve to estimate the encapsulation efficiency. The concentration of CUR was first determined by the calibration curve and the encapsulation efficiency (EE%) of the drug in the *Cur*-PDNCs was calculated by the total amount of *Cur* subtracting the residual *Cur* in the supernatant as illustrated in Equation (1)

$$EE\% = 1 - \frac{A}{B} \times 100\% \quad (1)$$

where *A* is defined as the amount of *Cur* out of the *Cur*-PDNCs; *B* is the total amount of *Cur* added in the initial process.[26]

To determin the behaviors of drug release behavior, free drug and *Cur*-PDNCs were dispersed and performed in dialysis bag (12.4 kDa pore size) in 5 mL release solution composed of 1% Dimethyl sulfoxide (DMSO) and 99% Dulbecco's modified Eagle's medium (DMEM). 1 mL of the release medium was collected periodically and replenished with 1 mL of release solution. *Cur* was extracted from the release media with mobile phase (35% $H_2O$ and 65% ACN). The quantity of *Cur* was determined by HPLC at the wavelength of 425 nm.

*PDNCs Modified with Lf*: *N*-(3-dimethylaminopropyl)-*N'*-ethylcarbodiimide (EDC) and *N*-hydroxysuccinimide (NHS) were used to crosslink the carboxylic acids and primary amines of the PDNCs. We added 100 μL EDC (0.1% in PBS, v/v) to the *Cur*-PDNCs solution for 30 min at room temperature (RT). The EDC was attacked by the carboxylic acid groups of the PDNCs to form an intermediate, which was unstable in aqueous solution and easily displaced by the nucleophile from primary amino groups in the liquid, named O-acylisourea. Subsequently, the particles were washed with PBS and centrifuged at 8500 rpm for 10 min. Subsequently, we added 5 mg Lf to the solution with vigorous stirring for 24 h at 4 °C. The product was formed by an amide bond that connected the primary amine and the original carboxyl group. A soluble urea derivative, which is an EDC by-product, was released. To improve the efficiency of the reaction, after mixing EDC and *Cur*-PDNCs, we added 100 μL NHS (0.1% in PBS, v/v)[27] because EDC would react with carboxyl groups on NHS to form an ester bonds that is more stable than O-acylisourea when connecting to primary amines. Finally, After rinsing with $H_2O$ and washed by PBS, Lf-*Cur*-PDNCs were prepared.[28]

*Cell Culture and Cell Cytotoxicity*: The Fischer-344 (F344) rat syngeneic GBM cell line RG2 (ATCC #CRL-2433) was purchased from Food Industry Research and Development Institute (FIRDI), Hsinchu, Taiwan. RG2 cells were cultured in DMEM containing 10% fetal bovine serum (FBS) and 1% penicillin-streptomycin. RG2 cells were cultured in complete medium at 37 °C in a humidified atmosphere of 5% carbon dioxide in air. The cytotoxicity was accessed by 3-(4, 5-dimethylthiazol-2-yl)-2, 5-diphenyltetrazolium bromide (MTT agent). Briefly, the RG2 cells were seeded in 24-well ($2 \times 10^4$ cells per well) and then treated with free drugs or drug nanocarriers at various concentrations and times. After the process, RG2 cells were incubated with 10% MTT agent for 4 h, and then the crystals in the bottom of the well were dissolved in DMSO before monitoring the absorbance by micro plate readers (ELISA reader, DV990BV4, GDV, Milan, Italy) at a wavelength 590 nm. Cell cytotoxicity and compatibility were determined and calculated by comparing untreated cells according to the following Equation (2)

$$\text{Cell viability } (\%) = \frac{\text{Absorbance of experimental group}}{\text{Absorbance of control group}} \times 100\% \quad (2)$$

*Determination of Cellular Uptake*: In order to estimate the cellular uptake of PDNCs as well as Lf-PDNCs, a total amount of $10^5$ RG2 cells were seeded and grew on glass coverslips for 24 h in 1 mL DMEM containing 10% FBS and 1% penicillin-streptomycin. The cells were cultured in complete medium at 37 °C in a humidified atmosphere of 5% carbon dioxide in air. After treated with PDNCs and Lf-PDNCs for 4 h, RG2 cells were washed in PBS twice and fixed for 30 min with 3% formaldehyde (PBS solution). Then, permeabilization was performed with 0.1% triton X-100 in PBS for 30 min and cells were washed in PBS twice. Finally, after staining with dihydrochloride (DAPI, 1 μg $mL^{-1}$) and F-actin (300 units $mL^{-1}$) for 30 min, respectively, the cells were mounted on fresh glass sides using mounting solution and observed under a fluorescence microscope.

The quantity of cellular uptake of the PDNCs was further confirmed by flow cytometry (Becton Dickinson, San Jose, CA, USA). RG2 cells were plated $2 \times 10^6$ in each well (6-well) and incubated with PDNCs and Lf-PDNCs for 4 h. After washing cells with PBS, we harvested the cells by trypsin-ethylenediaminetetraacetic acid (EDTA) buffer and resuspended in DMEM containing 10% FBS. Cells were collected through centrifugation at 1610 g for 5 min and resuspended in PBS for two times. Finally, we analyzed the quantity of cellular uptake with flow cytometry by accumulating $2 \times 10^4$ events.

*Animal Model and Implantation of RG2 Cells*: The protocol of animal use was reviewed and approved by the Institutional Animal Care and Use Committee (IACUC) of Tzu-Chi Hospital. F344 rats were purchased from the National Laboratory Animal Center (NLAC), Taipei, Taiwan, and bred in the Laboratory Animal Center of Tzu-Chi University for acclimatization at least 7 d before initiation of experiments. F344 rats (male, the bodyweight is 200–250 g) were anesthetized by intra-abdominal injection of diluted chloral hydrate (40 mg $mL^{-1}$) at a dose of 1 mL 100 $g^{-1}$ bodyweight. The head of the rat in prone position was fixed in the stereotactic frame (Lab Standard, Stoelting Corp., Wood Dale, IL, USA). Craniostomy was performed under the guidance of stereotactic frame with a target of 3 mm right and 3 mm behind the bregma. 500 RG2 cells in 10 μL solution was injected 4 mm deep into the brain via a 10 μL syringe at a rate of 1 μL $min^{-1}$. 10 min after completion of the injection, the syringe was slowly withdrawn, the craniostomy was sealed with bone wax, and the wound was closed with 3–0 nylon.

*Analysis of Plasma and Tumor Mass Cur Levels*: For comparison of the pharmacokinetic behaviors for different *Cur* formulations, 45 F344 brain-bearing rats (7 d after injecting cancer cells) were equally divided into three groups with the treatment of free *Cur*, *Cur*-PDNCs, and Lf-*Cur*-PDNCs via intravenously injecting, respectively. The dosage in

free *Cur* and *Cur*-PDNCs are equally 10 mg (the concentration of *Cur* is 33.3 mg $mL^{-1}$). The *Cur* concentration changes in blood plasma and brain tumor tissue were measured at 0.5, 6, 12, 24, and 72 h postinjection ($N = 3$ per time point) each group. The concentration of *Cur* were determined by HPLC with a UV detector set at the wavelength of 425 nm and mobile phase composed of 35% $H_2O$ and 65% ACN.

*In Vivo Antitumor Effect and Survival Study*: Thirty-six rats were used to evaluate both antitumor activity and survival analysis. On day 5 (postinjection with cancer cells), the tumor-bearing rats were randomly distributed into four groups (nine tumor-bearing rats per group). Three treatment groups were administered with intravenous injections of free *Cur*, *Cur*-PDNCs, and Lf-*Cur*-PDNCs, respectively, on day 5, 7, 9, 11, 13, and 15. The dosage of *Cur* in PDNCs and Lf-PDNCs was 12 mg $kg^{-1}$ and the concentration was equivalent to the dosage of free *Cur*. The control group was treated with normal saline. In this study, the tumor size was measured on day 21 because of statistical analysis consideration. Three animals were randomly picked to the histological analysis each group. The deeply anesthetized rats were perfused through the left ventricle with saline followed by 4% paraformaldehyde for animal sacrifice. Brains were removed and then were cut into 3 mm thick slices with a rat brain-cutting apparatus (#RBMS-600C, World Precision Instruments, Inc., Sarasota, FL, USA). The tumor volume was traced and the integrated volume was calculated using Image J software (NIH Image). Tumor volume was calculated by adding the region of interests (ROIs) of tumor areas for all histological sections and multiplying by slice thickness (3 mm).

*Statistics*: Data were expressed as mean ± SEM. Statistical significance was analyzed by Student's *t*-test. The survival analysis was done using the Kaplan–Meier method. $p < 0.05$ was considered to be statistically significant.

## Supporting Information

Supporting Information is available from the Wiley Online Library or from the author.

## Acknowledgements

This work was financially supported by National Chiao Tung University (NCTU), Ministry of Education, Aiming for the Top University Plan and the Ministry of Science and Technology of the Republic of China, Taiwan under Contract No. MOST 102-2221-E-010-011-MY3 and 102-2221-E-009-023-MY3. The authors thank 7T animal MRI Core Lab of the Neurobiology and Cognitive Science Center, National Taiwan University for technical and facility support.

Received: September 16, 2015
Revised: November 5, 2015
Published online: January 28, 2016

[1] S. C. J. Steiniger, J. Kreuter, A. S. Khalansky, I. N. Skidan, A. I. Bobruskin, Z. S. Smirnova, S. E. Severin, R. Uhl, M. Kock, K. D. Geiger, S. E. Gelperina, *Int. J. Cancer* **2004**, *109*, 759.

[2] L. Qiang, Y. Yang, Q.-D. You, Y.-J. Ma, L. Yang, F.-F. Nie, H.-Y. Gu, L. Zhao, N. Lu, Q. Qi, W. Liu, X.-T. Wang, Q.-L. Guo, *Biochem. Pharmacol.* **2008**, *75*, 1083.

[3] a) S. I. Pascu, R. L. Arrowsmith, S. R. Bayly, S. Brayshaw, Z. Y. Hu, *Philos. Trans. R. Soc. A* **2010**, *368*, 3683; b) M. Janssen, G. Mihov, T. Welting, J. Thies, P. Emans, *Polymers* **2014**, *6*, 799.

[4] M. Chapman, S. I. Pascu, *J. Nanomed. Nanotechnol.* **2012**, 2157.

[5] S. Kim, Y. Z. Shi, J. Y. Kim, K. Park, J. X. Cheng, *Expert Opin. Drug Deliv.* **2010**, *7*, 49.

[6] a) N. Mackiewicz, E. Gravel, A. Garofalakis, J. Ogier, J. John, D. M. Dupont, K. Gombert, B. Tavitian, E. Doris, F. Duconge, *Small* **2011**, *7*, 2786; b) E. Gravel, B. Theze, I. Jacques, P. Anilkumar, K. Gombert, F. Duconge, E. Doris, *Nanoscale* **2013**, *5*, 1955; c) J. Ogier, T. Arnauld, G. Carrot, A. Lhumeau, J. M. Delbos, C. Boursier, O. Loreau, F. Lefoulon, E. Doris, *Org. Biomol. Chem.* **2010**, *8*, 3902.

[7] a) F. Bonte, M. J. Hsu, A. Papp, K. Wu, S. L. Regen, R. L. Juliano, *Biochim. Biophys. Acta* **1987**, *900*, 1; b) G. S. Yu, H. Choi, Y. M. Bae, J. Kim, J. M. Kim, J. S. Choi, *J. Nanomed. Nanotechnol.* **2008**, *8*, 5266.

[8] a) D. Charych, J. Nagy, W. Spevak, M. Bednarski, *Science* **1993**, *261*, 585; b) C. X. Guo, P. Boullanger, T. Liu, L. Jiang, *J. Phys Chem. B* **2005**, *109*, 18765.

[9] J. Ravindran, S. Prasad, B. B. Aggarwal, *AAPS J.* **2009**, *11*, 495.

[10] a) M. M. Gottesman, I. Pastan, *Annu. Rev. Biochem.* **1993**, *62*, 385; b) R. Misra, S. K. Sahoo, *Mol. Pharm.* **2011**, *8*, 852; c) M.-C. Perry, M. Demeule, A. Régina, R. Moumdjian, R. Béliveau, *Mol. Nutr. Food Res.* **2010**, *54*, 1192; d) B. S. De Juan, H. Von Briesen, S. E. Gelperina, J. Kreuter, *J. Drug Target.* **2006**, *14*, 614; e) T. Ohnishi, I. Tamai, K. Sakanaka, A. Sakata, T. Yamashima, J. Yamashita, A. Tsuji, *Biochem. Pharmacol.* **1995**, *49*, 1541.

[11] P. D. Jeffrey, M. C. Bewley, R. T. A. MacGillivray, A. B. Mason, R. C. Woodworth, E. N. Baker, *Biochemistry* **1998**, *37*, 13978.

[12] a) L. Recht, C. O. Torres, T. W. Smith, V. Raso, T. W. Griffin, *J. Neurosurg.* **1990**, *72*, 941; b) W. M. Pardridge, J. Eisenberg, J. Yang, *Metabolism* **1987**, *36*, 892.

[13] a) J. Fang, H. Nakamura, H. Maeda, *Adv. Drug Deliver. Rev.* **2011**, *63*, 136; b) T. Stylianopoulos, *Ther. Deliv.* **2013**, *4*, 421; c) H. Kobayashi, R. Watanabe, P. L. Choyke, *Theranostics* **2013**, *4*, 81; d) R. A. Petros, J. M. DeSimone, *Nat. Rev. Drug Discov.* **2010**, *9*, 615.

[14] D. J. Ahn, J. M. Kim, *Acc. Chem. Res.* **2008**, *41*, 805.

[15] A. Yanagida, T. Kanda, T. Takahashi, A. Kamimura, T. Hamazono, S. Honda, *J. Chromatogr. A* **2000**, *890*, 251.

[16] C. Guo, S. Liu, C. Jiang, W. Li, Z. Dai, H. Fritz, X. Wu, *Langmuir* **2009**, *25*, 13114.

[17] a) D. J. Ahn, S. Lee, J.-M. Kim, *Adv. Funct. Mater.* **2009**, *19*, 1483; b) S. Kolusheva, R. Zadmard, T. Schrader, R. Jelinek, *J. Am. Chem. Soc.* **2006**, *128*, 13592.

[18] H. Xie, Y. Zhu, W. Jiang, Q. Zhou, H. Yang, N. Gu, Y. Zhang, H. Xu, H. Xu, X. Yang, *Biomaterials* **2011**, *32*, 495.

[19] a) G. P. Lim, T. Chu, F. Yang, W. Beech, S. A. Frautschy, G. M. Cole, *J. Neurosci.* **2001**, *21*, 8370; b) B. Ray, S. Bisht, A. Maitra, A. Maitra, D. K. Lahiri, *J. Alzheimers Dis.* **2011**, *23*, 61.

[20] Y. J. Wang, M. H. Pan, A. L. Cheng, L. I. Lin, Y. S. Ho, C. Y. Hsieh, J. K. Lin, *J. Pharmac. Biomed.* **1997**, *15*, 1867.

[21] R. A. Sharma, A. J. Gescher, W. P. Steward, *Eur. J. Cancer* **2005**, *41*, 1955.

[22] M. M. Yallapu, M. Jaggi, S. C. Chauhan, *Drug Discov. Today* **2012**, *17*, 71.

[23] L. Lv, Y. Shen, J. Liu, F. Wang, M. Li, M. Li, A. Guo, Y. Wang, D. Zhou, S. Guo, *J. Biomed. Nanotechnol.* **2014**, *10*, 179.

[24] S. H. Sun, H. Zeng, D. B. Robinson, S. Raoux, P. M. Rice, S. X. Wang, G. X. Li, *J. Am. Chem. Soc.* **2004**, *126*, 273.

[25] C. J. Pan, J. J. Tang, Y. J. Weng, J. Wang, N. Huang, *J. Control. Release* **2006**, *116*, 42.

[26] N. Suwannateep, W. Banlunara, S. P. Wanichwecharungruang, K. Chiablaem, K. Lirdprapamongkol, J. Svasti, *J. Control. Release* **2011**, *151*, 176.

[27] P. R. Edwards, A. Gill, D. V. Pollardknight, M. Hoare, P. E. Buckle, P. A. Lowe, R. J. Leatherbarrow, *Anal. Biochem.* **1995**, *231*, 210.

[28] G. K. Kouassi, P. Wang, S. Sreevatan, J. Irudayaraj, *Biotechnol. Progr.* **2007**, *23*, 1239.